Geomorphology 197 (2013) 156–169

Contents lists available at SciVerse ScienceDirect

Geomorphology

journal homepage: www.elsevier.com/locate/geomorph

Geomorphic effects, flood power, and channel competence of a catastrophic flood in confined and unconfined reaches of the upper Lockyer valley, southeast Queensland, Australia

Chris Thompson [a,b,*], Jacky Croke [b]

[a] Centre for Integrated Catchment Assessment and Management (ICAM), The Australian National University, Canberra ACT 0200, Australia
[b] Australian Rivers Institute, Griffith University Nathan Campus, Queensland 4111, Australia

ARTICLE INFO

Article history:
Received 22 August 2012
Received in revised form 10 May 2013
Accepted 13 May 2013
Available online 19 May 2013

Keywords:
Catastrophic flood
Geomorphic response
LiDAR
Stream power
Modelling

ABSTRACT

Flooding is a persistent natural hazard, and even modest changes in future climate are believed to lead to large increases in flood magnitude. Previous studies of extreme floods have reported a range of geomorphic responses from negligible change to catastrophic channel change. This paper provides an assessment of the geomorphic effects of a rare, high magnitude event that occurred in the Lockyer valley, southeast Queensland in January 2011. The average return interval of the resulting flood was ~2000 years in the upper catchment and decreased to ~30 years downstream. A multitemporal LiDAR-derived DEM of Difference (DoD) is used to quantify morphological change in two study reaches with contrasting valley settings (confined and unconfined). Differences in geomorphic response between reaches are examined in the context of changes in flood power, channel competence and degree of valley confinement using a combination of one-dimensional (1-D) and two-dimensional (2-D) hydraulic modelling. Flood power peaked at 9800 W m^{-2} along the confined reach and was 2–3 times lower along the unconfined reach. Results from the DoD confirm that the confined reach was net erosional, exporting ~287,000 m^3 of sediment whilst the unconfined reach was net depositional gaining ~209,000 m^3 of sediment, 70% of the amount exported from the upstream, confined reach. The major sources of eroded sediment in the confined reach were within channel benches and macrochannel banks resulting in a significant increase of channel width. In the unconfined reach, the benches and floodplains were the major loci for deposition, whilst the inner channel exhibited minor width increases. The presence of high stream power values, and resultant high erosion rates, within the confined reach is a function of the higher energy gradient of the steeper channel that is associated with knickpoint development. Dramatic differences in geomorphic responses were observed between the two adjacent reaches of contrasting valley configuration. The confined reach experienced large-scale erosion and reorganisation of the channel morphology that resulted in significantly different areal representations of the five geomorphic features classified in this study.

1. Introduction

Flooding is a persistent threat to both human life and infrastructure globally (Baker et al., 1988). Even modest changes in climate are thought to lead to large increases in flood magnitudes (Knox, 1993, 2000; Macklin and Lewin, 2003), the extent of which remains largely unknown in many parts of the world including Australia. Here, evidence of extreme flood magnitudes during the Pleistocene and Holocene has come from limited slackwater and paleostage studies in parts of northern and central Australia (Wohl, 1992; Nott and Price, 1999; Pickup et al., 2002; Jansen and Brierley, 2004). A number of studies have also reported on the magnitude and geomorphic change resulting from rare floods (~100-year average return interval: ARI) in populated parts of eastern Australia (e.g., Nanson, 1986; Erskine, 1993; Erskine and Saynor, 1996) over the last century that describe changes to channel geomorphology ranging from minor to catastrophic. The degree of change has been related to decadal shifts from drought- to flood-dominated regimes (Erskine and Warner, 1988, 1998; Warner, 1997), land use change (Brooks and Brierley, 1997; Kirkup et al., 1998), and a recent flood history that has preadjusted the channel such that subsequent threshold-exceeding events have less impact (Erskine, 2011).

Continuing research has advanced our understanding of the role of key drivers of geomorphic change such as flood power (Kale, 2008), flood competence (Jansen, 2006), sequencing of flood events (Magilligan et al., 1998), and spatial changes in valley floor configuration (Fuller, 2008; Cheetham et al., 2010). A review of these studies also suggests that the spatial scale of investigation may also influence interpretations of the geomorphic effectiveness of specific flood events

* Corresponding author at: Centre for Integrated Catchment Assessment and Management (ICAM), The Australian National University, Canberra ACT 0200, Australia. Tel.: +61 737357963.
E-mail address: Chris.Thompson@griffith.edu.au (C. Thompson).

0169-555X/$ – see front matter © 2013 Elsevier B.V. All rights reserved.
http://dx.doi.org/10.1016/j.geomorph.2013.05.006

with many conclusions derived from reach-scale planform change surveys and limited cross sections. Such approaches can limit detailed understanding of spatial changes in erosion and deposition processes and of the transfer or redistribution of material fluxes between reaches. It remains uncertain, therefore, if river reaches that experience dramatic geomorphic change are representative of the 'overall' geomorphic response or one end of the response spectrum that occurs in localised areas. The factors that may play a role in conditioning the system to a particular response are therefore often difficult to elucidate.

Recent technological advances now make it more tangible to address these issues across larger spatial scales. The increasing availability and use of high resolution topographic data has opened up the possibility of more rapid and spatially extensive assessments of flood-related geomorphic change. For example, Airborne LiDAR (light-induced direction and ranging) data are increasingly used in fluvial geomorphology, including the mapping of gravel-bed rivers (Charlton et al., 2003), defining the boundary layer for hydraulic modelling (French, 2003; Aggett and Wilson, 2009; Kermode et al., 2012), and determining channel heads and stream networks (Sun et al., 2011, 2012). The contribution of this technology over the more traditional at-a-site and planform surveys is unquestionable from a practical flood risk perspective and from improved understanding of spatial variability in geomorphic processes.

This paper presents an assessment of the geomorphic effects of a rare high magnitude event that occurred in the Lockyer valley, southeast Queensland (SEQ) in January 2011 using a combination of one- (1-D) and two-dimensional (2-D) flow hydraulic modelling and morphological budgeting using a multitemporal LiDAR-derived DEM of Difference (DoD). This study tests the hypothesis that differences in geomorphic response between the selected confined and unconfined reaches can be explained in terms of relative differences in flood power, channel competence, and degree of valley confinement.

2. Study area

The Lockyer valley falls to the east of the city of Toowoomba, which lies on the Great Dividing Range and marks the catchment divide from the Murray–Darling basin (Fig. 1). The Lockyer catchment drains nearly 3000 km^{2}of prime agricultural land in southeast Queensland (SEQ). Southeast Queensland is a subtropical region with mean maximum monthly temperatures ranging between 21 and 29 °C. The total annual rainfall ranges between 900 and 1800 mm, with the majority falling during the warm summer season (October to February) (Bureau of Meteorology, BoM, 2012). The region is characterised by seasonally variable patterns of floods and droughts that have been linked to the interannual rainfall variations of the El Niño–Southern Oscillation

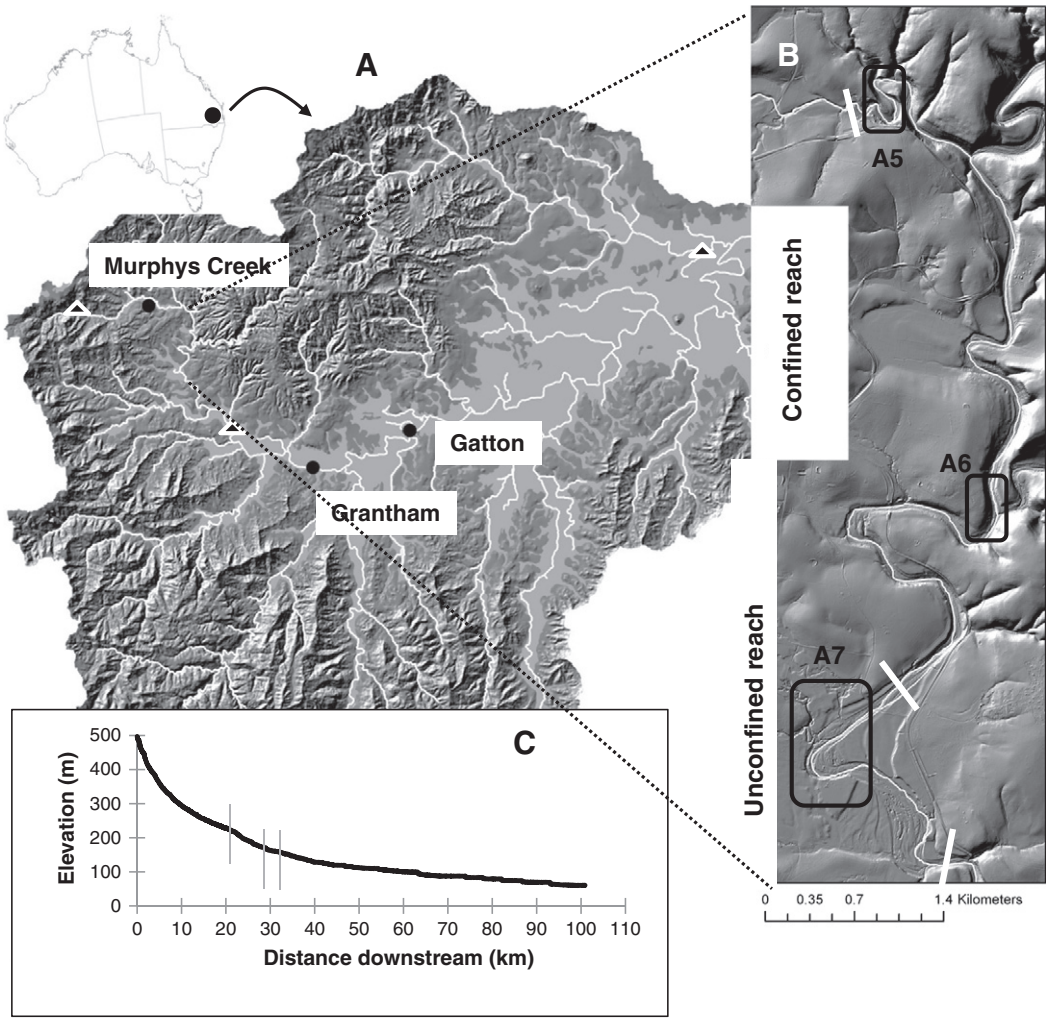

Fig. 1. The Lockyer catchment in eastern Australia showing (A) Gatton, the largest town in the catchment and the communities of Murphys Creek and Grantham that were severely impacted by the flood with numerous lives lost. The three triangles represent locations of gauging stations Spring Bluff (upper), Helidon (mid), and Rifle Range Road (lower catchment). (B) The location of the two adjacent study reaches is displayed on the LiDAR-derived DEM with field survey sites A5, A6, and A7 marked. (C) The longitudinal profile of Murphys and Lockyer Creeks with upper mark showing knickpoint and start of the confined reach, the transition into the unconfined reach, and final mark indicating the end of the study site.

(ENSO) and the Interdecadal Pacific Oscillation (IPO) (Kiem et al., 2003; Rustomji et al., 2009). Flash flood magnitude indices (FFMI) for major basins in SEQ range from 0.50 to 0.99, indicating a propensity for alternating extremes (Rustomji et al., 2009).

The catchment forms a typical bowl shape with the high elevation of the Ranges (700 to 800 m above sea level (asl)) in the west, draining to the wide alluvial plains in the lowlands. Tertiary volcanics persist on the top of the range, but give way to Jurassic Marburg Formation consisting of sandstone, siltstone, shale, and conglomerates (Whitaker and Green, 1980) in the headwaters that bisect steep forest terrain whilst flowing in an easterly direction. Below the township of Murphys Creek (Fig. 1), the channel passes through the more resistant and older (Triassic–Jurassic) Helidon sandstones. Here the channel, with a catchment area of 63 km^2, becomes confined and is forced to flow south around the edge of this geological unit, which has relatively low sinuosity with the exception of a couple of large meander bends. At Helidon, the creek resumes flowing in an easterly direction over Quaternary alluvial sediments into an expanding valley floodplain occupied by intensive agriculture, predominantly irrigated vegetable cropping.

2.1. Selected study reaches

Two reaches of contrasting valley setting were selected for detailed study: a confined and an adjacent unconfined reach located in the upper Lockyer catchment between the towns of Murphys Creek and Helidon (Fig. 1). Within the two study reaches are three field survey sites (A5, A6, and A7) (Fig. 1B).

2.2. Confined reach

The confined reach is located below the township of Murphys Creek where the channel contacts the Helidon sandstones and is forced to flow south. The start of the reach has a catchment area of 63 km^2. The average bed gradient increases from 0.0053 m m^{-1} above the confined reach to 0.0065 m m^{-1} marking the location of a knickpoint. Two main tributaries, Fifteen Mile Creek (91 km^2) and Alice Creek (60 km^2), join along this reach resulting in a total catchment area of 237 km^2. The 9-km-long confined reach is predominantly a bedrock channel with a coarse alluvial cover. The channel flows between hills of native eucalypt woodland/forest. The reach has an entrenchment ratio of around 1.3, which is 12 times less than that measured upstream of the confined reach.

2.3. Unconfined reach

The second reach is located immediately downstream of the confined reach where the channel exits the confining bedrock and develops a more sinuous planform contributing to a total catchment area of 256 km^2. The total reach length is 3 km and is characterised primarily by a large meander loop (Fig. 1). Channel bed gradient reduces to an average of 0.0008 m m^{-1}, and the entrenchment ratio increases to 25 reflecting the widening of the valley floor and more continuous floodplain development. The floodplains have been cleared for stock grazing and some cropping.

3. The January 2011 event

3.1. The storm

A detailed synopsis of the events' meteorology and hydrology is provided by Jordan (2011). In summary, a strongly La Niña event lead to a wet summer; and in the days leading to the event, 20 to 30 mm had fallen across the catchment. On 10 January 2011, the soils were already saturated when a number of massive storm cells converged and moved across the top of the catchment and intensified further from the orographic effect. The area covered by the converged storm cells was approximately equal to the entire Murphys Creek catchment (237 km^2). Peak two-hour rainfall intensities had annual exceedance probabilities (AEP) that ranged from 1 in 18 years in the west to 1 in 1088 years in the north of the upper catchment (Rogencamp and Barton, 2012).

3.2. The flood

The approximate magnitude of the January 2011 event was captured by the gauging stations along the course of the mainstem until they failed near the flood peak (Jordan, 2011). Peak discharges are presented in Table 1, resulting in average transmission speeds of 24.2 km h^{-1} between Spring Bluff and Helidon gauges and 2.9 km h^{-1} between Helidon and Rifle Range Road gauges. Whilst uncertainty exists in these absolute values based on upper tributary contributions, the relative change shows a stark difference between the upper and lower Lockyer catchment in terms of flood wave propagation and magnitude. The slowing flood wave speed and diminishing flood peak indicate that most of the runoff was derived from the steeper headwaters.

The average return interval (ARI) of the January flood based on the Log Pearson type III (LP3) analysis of the annual flood series was found to be around 2000 years at Spring Bluff gauge, around 400 years at Helidon (~36 km downstream), and 27 years at the Rifle Range Road gauge (~73 km farther downstream) (Table 1). These estimates of event ARI are based on LP3 yield similar values to the statistical metrics calculated by Rustomji et al. (2009) and are applied to the annual maximum flood series and the flood peaks-over-threshold data. Rogencamp and Barton (2012) modelled a higher peak discharge at the Helidon gauge for the flood peak and suggested it represented a 2000-year ARI.

4. Methods

4.1. Field assessment

A field geomorphic assessment of the study reaches was undertaken post the event in May 2011. Three sites (A5, A6, A7) were investigated in detail with each site consisting of ~10 transects spaced roughly 100 m apart and surveyed perpendicular to the main channel (Fig. 1B). Field estimates of channel geometry (channel width, bank inclination, and height) were obtained using a TruPulse™ hand-held laser scanner. An approximate estimate of water depth at each site was obtained using a depth ranging rod. The 10 largest boulders on the channel bed were measured across their intermediate (*b*-axis) in the confined reach to provide data for the hydraulic models and competence equations. Given the size of the boulders, their resting angle, and partial burial in the channel bed, measurements of the *b*-axes for some boulders required some approximation.

Table 1
Flood characteristics.

Flood/gauge attributes	Spring Bluff GS 143219A	Helidon GS 143203C	Rifle Range Road GS 143210B
Length of record (y)	31	24	24
Catchment area (km^2)	18	357	2490
FFMI	0.88	0.7	0.68
Q_p gauged (m^3 s^{-1})	361.5	3642	1453
Specific peak discharge (m^3 s^{-1} km^{-2})	20.08	11.76	0.58
Q_p/MAF	15.1	10.9	4.5
[a]Recurrence interval (y)	~2000	100	27

[a] Calculated from Log Pearson type 3 analyses of annual maximum flood series.

4.2. Sequential high resolution LiDAR and aerial photography surveys

LiDAR and near-coincident high resolution aerial photography was acquired for ~1300 km^2 over the Lockyer valley in August–October 2010 and again immediately following the flood in February 2011 by the Queensland's Department of Environment and Natural Resource Management (QDERM). The pre-flood capture was acquired with a Lexica ALS50-11 Airborne Laser Scanner at an average point density of 2 points/m^2. Post-flood LiDAR was captured in January 2011 using a Riegl LMS-Q680 airborne laser scanner at ~4 points/m^2.

Survey points were filtered to remove any visually obvious anomalies before deriving a triangular irregular network (TIN) using Delaunay triangulation for both LiDAR captures. The resultant pre- and post-flood DEMs were differenced by subtracting the elevations in each DEM on a cell-by-cell basis to produce a DoD.

4.3. LiDAR error assessment

The process of accounting for DoD uncertainty requires three main steps (Wheaton et al., 2010) consisting of (i) quantifying the surface representation uncertainty in the individual DEM surfaces; (ii) propagating the identified uncertainties into the DoD; and (iii) assessing the significance of propagated uncertainty. These were investigated here as follows.

4.3.1. Quantifying surface representation uncertainty

The most commonly adopted procedure for managing DEM uncertainties involves specifying a minimum level of detection threshold ($_{min}LoD$) to distinguish actual surface changes from inherent noise (Fuller et al., 2003). Typically this is addressed by applying the classical theory of errors (Taylor, 1997), taking a measure of DEM precision derived from check data as a surrogate for DEM quality. This information was provided by AAM for the pre-flood LiDAR DEM with a reported root mean square error (RMSE) of 0.08 m with a standard deviation of error (SDE) of 0.15 m based on comparison of the pre-flood DEM with GPS survey points on hard surfaces. For the post-flood capture, this study quantified DEM uncertainty using an existing statewide, permanent survey control database. A total of 286 survey marks (SMs), excluding any known to be in poor condition or buried as a result of the flood, were used and produced a mean height difference of 0.08 m and SDE of 0.17 m.

4.3.2. Propagating uncertainty into the DoDs

Brasington et al. (2003) and Wheaton et al. (2010) demonstrated that individual errors in the DEM can be propagated into the DoD as

$$\delta u_{DoD} = \sqrt{(\delta z_{new})^2 + (\delta z_{old})^2} \quad (1)$$

where δu_{DoD} is the propagated error in the DoD, and δz_{new} and δz_{old} are the individual errors in DEM_{new} and DEM_{old}, respectively. The method assumes that errors in each cell are random and independent. Using the SDE values as estimates of δz, the combined error was calculated as a single value of ± 0.23 m for the entire DoD.

4.4. Reach geomorphic classification

The areal representation of geomorphic features within the selected reaches was classified using a 1-D step backwater model HEC-RAS and terrain slope thresholds. Full details of the model setup are provided in Croke et al. (2013) but in brief, five main geomorphic types were differentiated based on pre-flood topography: (i) inner channel bed and bars, (ii) inner channel banks, (iii) benches, (iv) macrochannel banks, and (v) floodplain and/or terrace. The valley bottom or floodplain extent was defined by applying Gallant and Dowling's (2003) valley bottom flatness index (MrVBF) with an index of 3 used to best differentiate the floodplain from the remaining catchment area. Hydraulic modelling of the 2.33 return interval event ($Q_{2.33}$) and bankfull (Q_{bf}) was used to derive raster analysis masks within the floodplain area for further classification into geomorphic types. The $Q_{2.33}$ inundation extent modelled by HEC-RAS showed good demarcation between the most active part of the channel (the inner channel) bound by short, steep banks with little or no vegetation, and the bank-tops lined with perennial riparian vegetation [*Callistemon sp.*]. Within the $Q_{2.33}$ mask area, a terrain slope of 10° differentiated channel bed topography from channel banks. The Q_{bf} inundation extent modelled by HEC-RAS delineated the macrochannel area from surrounding valley bottom. Subtracting the $Q_{2.33}$ area from the Q_{bf} area provided an analysis mask for identifying macrochannel banks and within channel benches. These features were differentiated by a terrain slope of 14°. The subtraction of the Q_{bf} — macrochannel area from the valley bottom area leaves the area occupied by floodplain and terraces. Slopes that exceeded 14° were classified as macrochannel bank, allowing for the inclusion of bank tops not included in the Q_{bf} zone because of one bank being higher than the adjacent side. This also included some steep slopes between floodplain and terraces however; these slopes were not continuous to allow classification of terrace units. The percentage area occupied by each feature was determined using shapefiles post-processed within ArcGIS.

4.5. Estimates of net volumetric changes

Using each shapefile, elevation difference data were extracted from the DoD at 5 cm height intervals. Estimates of net volumetric change were approximated using a simple integration scheme, multiplying the calculated elevation change (a depth measurement in metres) by surface area of each cell (1 m^2). Volumes were then summed into 'cut' or erosion and 'fill' or depositional categories to produce a net volumetric budget for each geomorphic feature. Because of the presence of water in the inner channel unit in the post-flood capture, a water surface mask was applied to eliminate these areas in comparative budget estimates.

4.6. Hydraulic modelling of flood peak

Hydraulic modelling was undertaken to calculate flood power, boundary shear stress, and competence for the January 2011 flood peak. A 2-D hydraulic model TUFLOW (Syme and Apelt, 1990) was applied as part of the flood risk management study for the Lockyer Valley Regional Council (Rogencamp and Barton, 2012; SKM, 2012). TUFLOW has been rigorously tested for flood modelling in catchments containing urban settings and has produced reliable results (Hunter et al., 2008; Fewtrell et al., 2011). TUFLOW was re-run for this study within the designated reaches to maintain consistency between results reported in the flood risk management study (SKM, 2012) and this work.

The model was constructed as a dynamically linked 1-D/2-D model with varying grid size for the greater Lockyer Creek catchment. For this study, only the upper catchment single 2-D domain was run using a 7-m grid cell resolution. The hydrologic model XP-RAFTS was used for runoff routing and deriving the input hydrographs for TUFLOW. The catchment was delineated into 10 km^2 subcatchments for calculating excess rainfall, slope, roughness, and land use. Land use served to determine percentage pervious and impervious surface. Roughness was based on Manning's n with values given in Table 2. Rainfall was derived from the Australian Bureau of Meteorology radar images to yield hourly rainfall patterns for each subcatchment. Rainfall loss parameters were determined through calibration with gauged stream flow for the event (Table 2). The resulting subcatchment hydrographs were routed through the drainage system using the Muskingum-Cunge method.

Table 2
Values used in XP-RAFTS and TUFLOW models.

Parameter	Attribute/variable	Value
Manning's n	Low-medium dense vegetation	0.1
	Dense vegetation	0.17
	Other riparian vegetation	0.08
	Channel banks	0.1
	Inner channel	0.06
	Bare/fallow ground	0.04
	Pasture	0.04
	Impervious surface	0.02
Rainfall loss	Initial loss	10 mm
	Continuing loss	2 mm
	Storage coefficient	0.8
	Storage exponent	0.4

The calibrated XP-RAFTS hydrographs were used as input data for TUFLOW. In TUFLOW, hydraulic roughness is also based on Manning's n (Table 2). The downstream boundary condition was a stream gauged water level located 7 km downstream of the study reaches. The modelled water level and discharge for the flood event was calibrated against gauged stream flow. The modelled flood peak was within 0.2 m of surveyed trash lines and gauged levels (Rogencamp and Barton, 2012; SKM, 2012).

Output data for each grid cell in TUFLOW include water depth and average velocity. These are used in the model to calculate bed shear stress (τ_b) (Eq. (2)) and flood power (ω_p) (Eq. (3)) for the flood peak flow.

$$\tau_b = \frac{\rho g V^2 n^2}{y^{1/3}} \quad \left(\text{kg m}^{-1}\ \text{s}^{-2}\right) \tag{2}$$

$$\omega_p = |V|\tau_b \quad \left(\text{W m}^{-2}\right) \tag{3}$$

where ρ is the density of water, g is the gravity, V is the velocity, n is the Manning's roughness, and y is the water depth over the grid cell.

4.7. Competence prediction

The TUFLOW model results for flood power and bed shear stress are used to calculate the maximum grain size that could be transported based on three selected equations.

Costa's (1983) critical unit stream power regression model,

$$D_{reg} = \left(\frac{\omega}{0.03}\right)^{1/1.686} \quad (\text{mm}). \tag{4}$$

Costa's (1983) lower envelope curve for critical unit stream power derived from empirical data from catastrophic floods,

$$D_{lec} = \left(\frac{\omega}{0.009}\right)^{1/1.686} \quad (\text{mm}). \tag{5}$$

Shield's entrainment equation, which has previously been applied to determine flood competence (e.g., Phillips, 2002),

$$D_{Shields} = \frac{\tau_b}{[\tau_c^*(\rho_s - \rho)g]} \quad (\text{m}) \tag{6}$$

where s is the energy gradient derived from the 2-D hydraulic model, τ_c^* is the critical shear stress and set to 0.06, τ_b is the modelled boundary shear stress, ρ_s is the density of the rock/boulder, ρ is the density of water, and g is the gravity.

Eq. (6) was originally derived for uniform spherical grains; however, our lack of data for pre-flood grain size distribution and bedform configurations prevents consideration of grain-size scaling (cf Andrews, 1983) as previously used by Bathurst (1978), Komar (1987), and Ferguson (2005).

5. Results

5.1. Geomorphic setting

All geomorphic types are represented in both reaches, but the geomorphic classification results show strong departures between the two reaches in terms of their relative aerial coverage (Fig. 2). The dominant features along the confined reach are the macrochannel banks and benches. The floodplain is largely absent along the straight

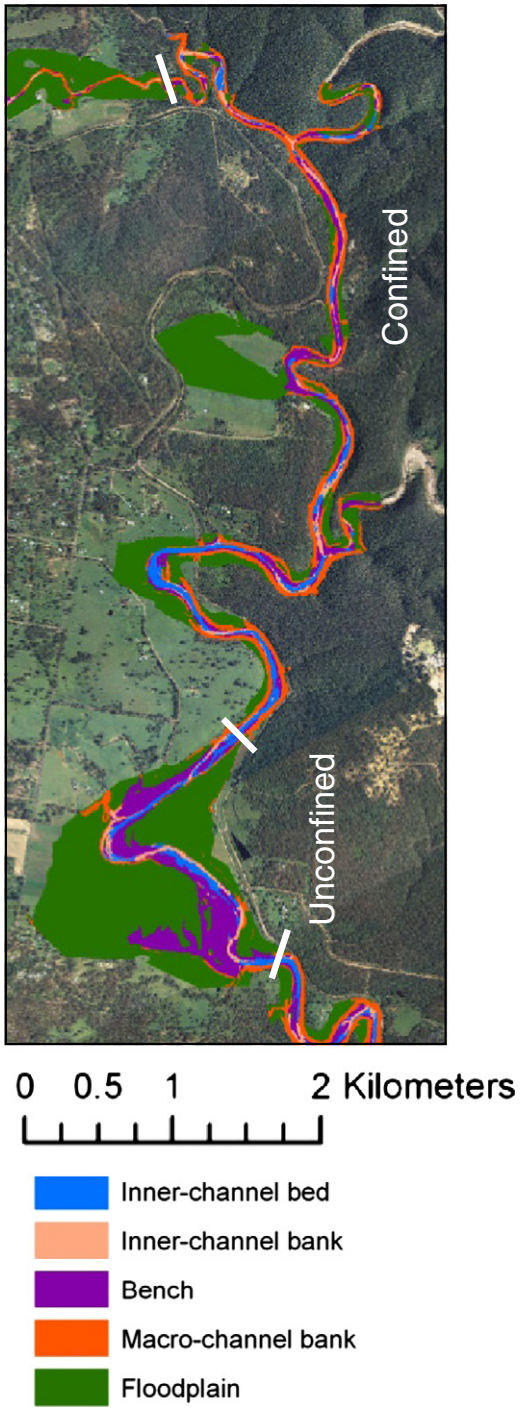

Fig. 2. The distribution of classified geomorphic types along the study reaches based on pre-flood topography.

sections of the confined reach with some discrete floodplain 'pockets' located on the inside of bends and at the tributary junctions. Benches are a relatively continuous feature along the confined reach alternating between the left and right side of the channel. In contrast, the unconfined reach is dominated by floodplain and benches comprising over 75% of the total area. Benches along the unconfined reach run along both sides of the channel. The inner channel banks occupy the least area along both reaches.

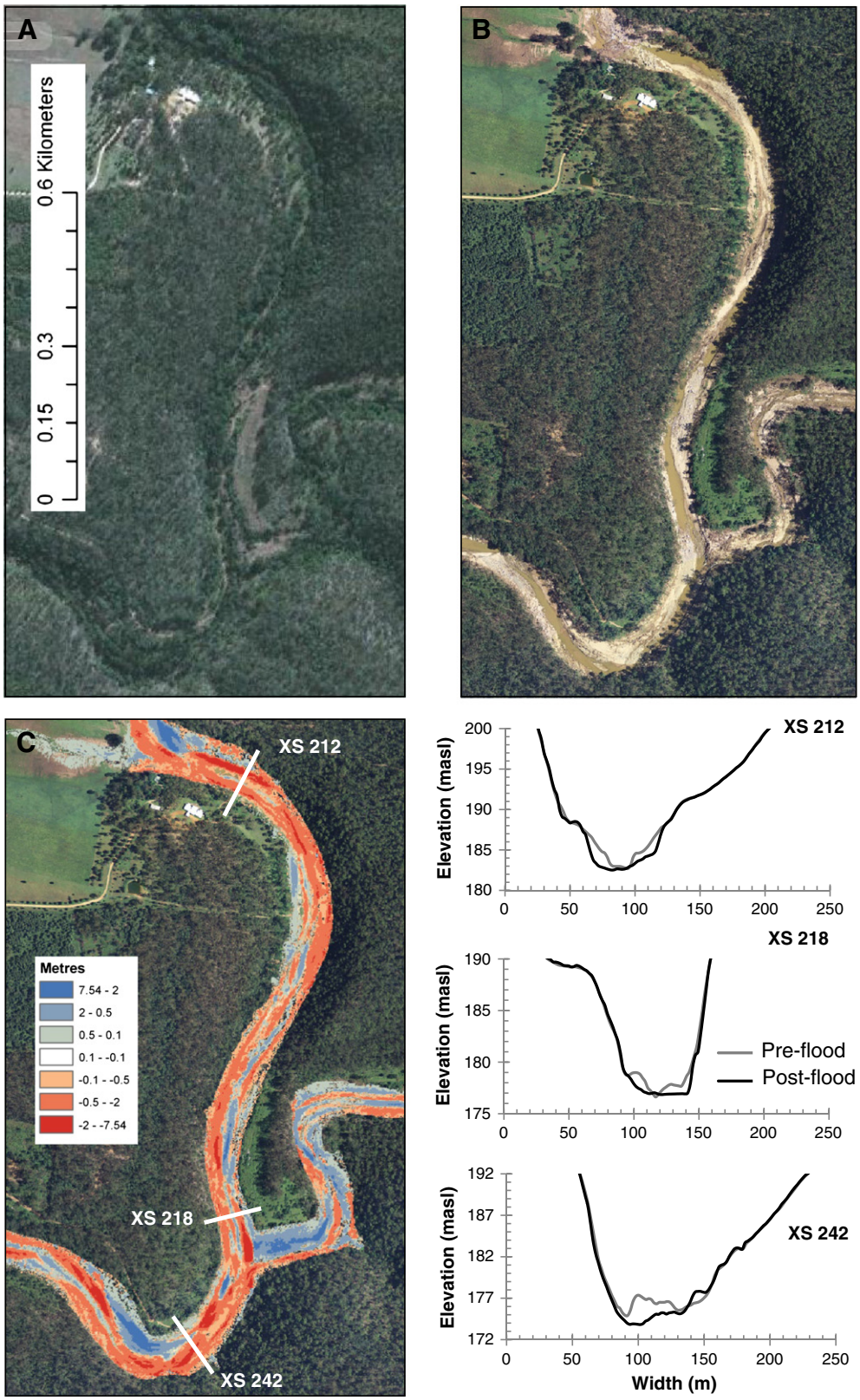

Fig. 3. Change along the confined reach with (A) showing pre-flood aerial photos (July 2009), (B) post-flood aerial photos, (C) elevation change from DoD, and (D) differences in cross section geometry from representative XS interpolated from LiDAR DEM.

Table 3
Geomorphic features and there change during the January flood: positive values indicate deposition and negative values indicate erosion.

Reach	Feature	Pre-flood area (ha (%))	Depth change (m) (incl. water)	Volume (m^3) (incl. water)	Volume[a] (m^3) (excl. water)	Post-flood area (%)
Confined	Inner channel	11.9 (16)	0.06	6977	11,913	35
	Inner channel banks	10.1 (14)	−0.23	−23,717	−6986	6
	Bench	17.5 (24)	−0.85	−148,173	−10,745	17
	Macrochannel banks	21.2 (29)	−0.51	−107,117	−93,457	26
	Floodplain	12.8 (17)	−0.12	−15,014	−12,370	16
	Mean		−0.33			
	Sum	73.5		−287,044	−202,645	
Unconfined	Inner channel	7.3 (7)	0.71	51,556	40,768	11
	Inner channel banks	4.7 (4)	0.80	37,270	33,010	1
	Bench	30.5 (29)	0.2	60,883	72,679	42
	Macrochannel banks	7.0 (7)	0.1	6606	7929	6
	Floodplain	56.5 (53)	0.09	52,504	59,937	40
	Mean		0.20			
	Sum	105.9		208,820	214,322	

[a] Decrease in eroded volume owing to post-flood water extent occupying areas that were originally banks and benches that were stripped during the flood event. See Section 5.2 for further details.

5.2. Geomorphic responses in the two reaches

As illustrated in the pre- and post-flood aerial photos, significant channel change occurred along the confined reach (Fig. 3A, B) where pre-flood consisted of an almost imperceptible channel amidst dense riparian vegetation that was subsequently removed by the flood. Table 3 summarises changes to the areal extent of each of the four geomorphic features classified and highlights the dramatic change in the width of the post-flood inner channel that ranged from 13 to 360%. The cross sections highlight spatial variability with some sites showing pronounced incision whilst others displayed no change in bed elevation (Fig. 3D, E). Estimates of erosion and deposition derived from the DoD confirm that this confined reach was net erosional with a net loss of 287,044 m^3 of sediment (Table 3). In general, all geomorphic features are net erosional with the benches providing the dominant source of eroded material (148,000 m^3) (Table 3). The inner channel area experienced infilling by deposition; however, this estimate is compounded by water in the post-flood channel. When water is excluded from the analyses, 85,000 m^3 less sediment is shown to be removed. This results because a large area of the post-flood water mask overlies areas that were originally inner channel banks, benches, and even the bases of macrochannel banks. Ignoring these areas would result in gross underestimation of net erosion.

The calibre of eroded material consisted predominantly of sand, gravel, cobbles, and boulders (Fig. 4A, B) with field-derived estimates of average intermediate *b*-axes of the largest boulders approaching 2 m.

In the unconfined reach, comparison of pre-flood to post-flood aerial photos highlighted the large amount of sediment deposition on the floodplain and benches (Fig. 5) with evidence of lateral channel expansion and the development of a new flood chute across the bend. Differences in pre- to post-flood channel width ranged from 0 to 75% with channel cross sections typically showing infilling of the inner channel (e.g., Fig. 5D). Major changes were observed in the proportional area of inner channel banks, which decreased to just 1% of total area after the flood (Table 3).

Estimates of erosion and deposition from the DoD indicate that this reach was net depositional, with the DoD clearly demarcating areas of cut from fill across the floodplain/bench features (Fig. 5C). For example, estimates of −2 m elevation differences were recorded in the vicinity of the road crossing scour hole and flood chute. In contrast, a similar elevation gain of +2 m was estimated across the benches and floodplain on the lee side of the bend (Table 3). Benches accumulated the most sediment out of the geomorphology types along the reach (Table 3) with the calibre of deposited sediment, ranging from sand-gravel material (Fig. 5A) with evidence of some small boulders with *b*-axes up to 300 mm deposited halfway across the floodplain.

5.3. Flood power

Fig. 6A and B illustrates the range of unit flood power values predicted using TUFLOW for representative areas of the two reaches. The confined reach shows unit flood power values in the 1000–3000 W m^{-2} range along the centre of the channel with patches in the 5000–10,000 W m^{-2} range along the macrochannel bank. The highest mean and 95th percentile (+2σ) unit flood power values were recorded along the macrochannel banks followed by the inner channel, banks, and bench (Table 4).

Along the unconfined reach, high unit flood power values were evident leading into the reach and a patch mid-reach in the 1000–3000 W m^{-2} range, whilst the remainder of the reach experienced

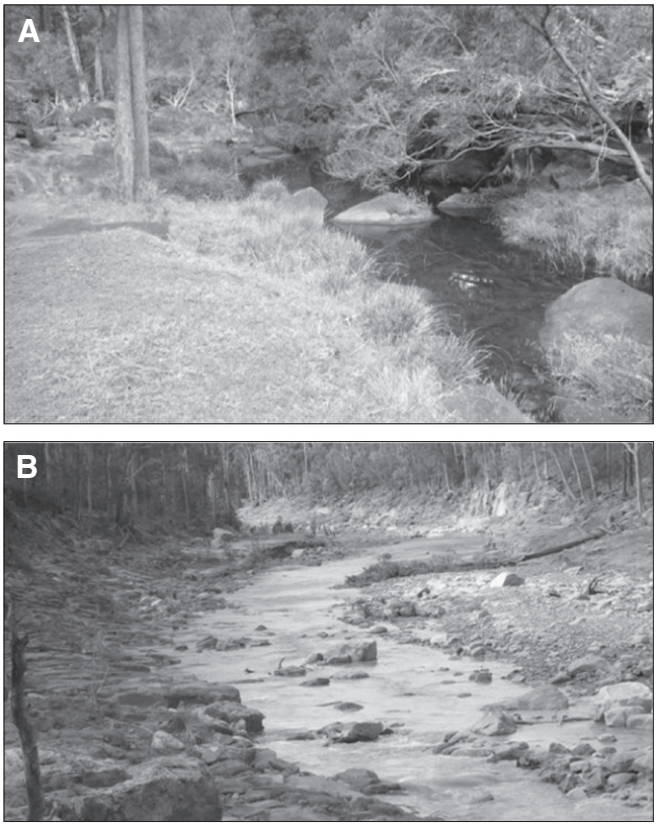

Fig. 4. Photographs from middle of confined reach taken (A) in the year before the flood and (B) in the days after the January 2011 flood.
Source: Murphy's Creek Escape (www.murphyscreekescape.com.au).

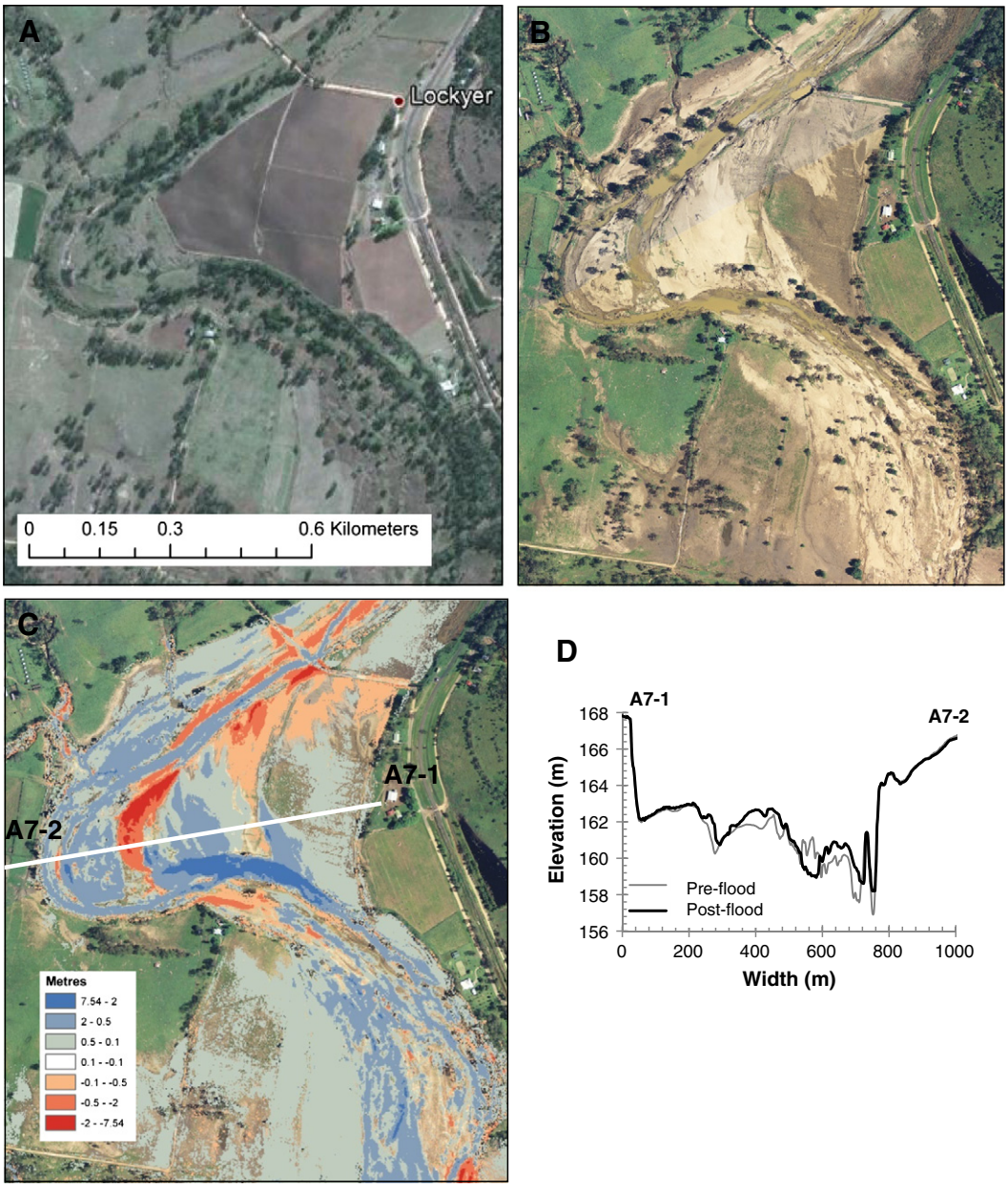

Fig. 5. Change along unconfined reach showing (A) pre-flood aerial photos (July 2009), (B) post-flood aerial photos, (C) elevation change from DoD, and (D) difference in cross section geometry.

lower flood power. The macrochannel banks and inner channel experienced the highest mean flood power, followed by the inner channel bank (Table 4). Benches had a mean flood power of 347 W m^{-2}, whilst the floodplains had an average of 180 W m^{-2}.

5.4. Flood competence

Results of the flood competence equations used in this study represent the largest predicted grain size mobilised during the flood peak based on the mean and the 95th percentile ($+2\sigma$) flood power modelled across each geomorphology feature (Fig. 7). The mean and largest grain sizes predicted by D_{reg} (Eq. (4)) fall below the field-measured boulders of 2 m in the confined reach.

D_{lec} (Eq. (5)) predicts a mean boulder size of 1.3 m and a 2σ grain size of ~2.4 m across the inner channel, banks, and benches (Fig. 7). This upper limit grain size encapsulates the field-measured boulder sizes along the post-flood inner channel bed. The predicted maximum (2σ) grain sizes along the macrochannel are over 3 m.

$D_{Sheilds}$ (Eq. (6)) produced similar results to D_{reg} for the inner channel, banks and bench areas but increased significantly to be comparable to D_{lec} for the macrochannel banks and floodplain areas along the confined reach. Based on the comparisons with field estimates of boulder sizes known to have been mobilised during the flood (e.g., Fig. 4A, B), D_{reg} and $D_{Sheilds}$ underpredict flood competence whilst D_{lec} is a better predictor of flood competence.

Results of competence modelling across the unconfined reach show similar trends between the three equations; however, predicted grain size is at least 50% smaller. Field measurements of post-flood deposits of cobbles and small boulders with *b*-axes of up to 300 mm across the first half of the floodplain of the inner bend provide a guide to the point at which floodwaters lost competence to transport these grains.

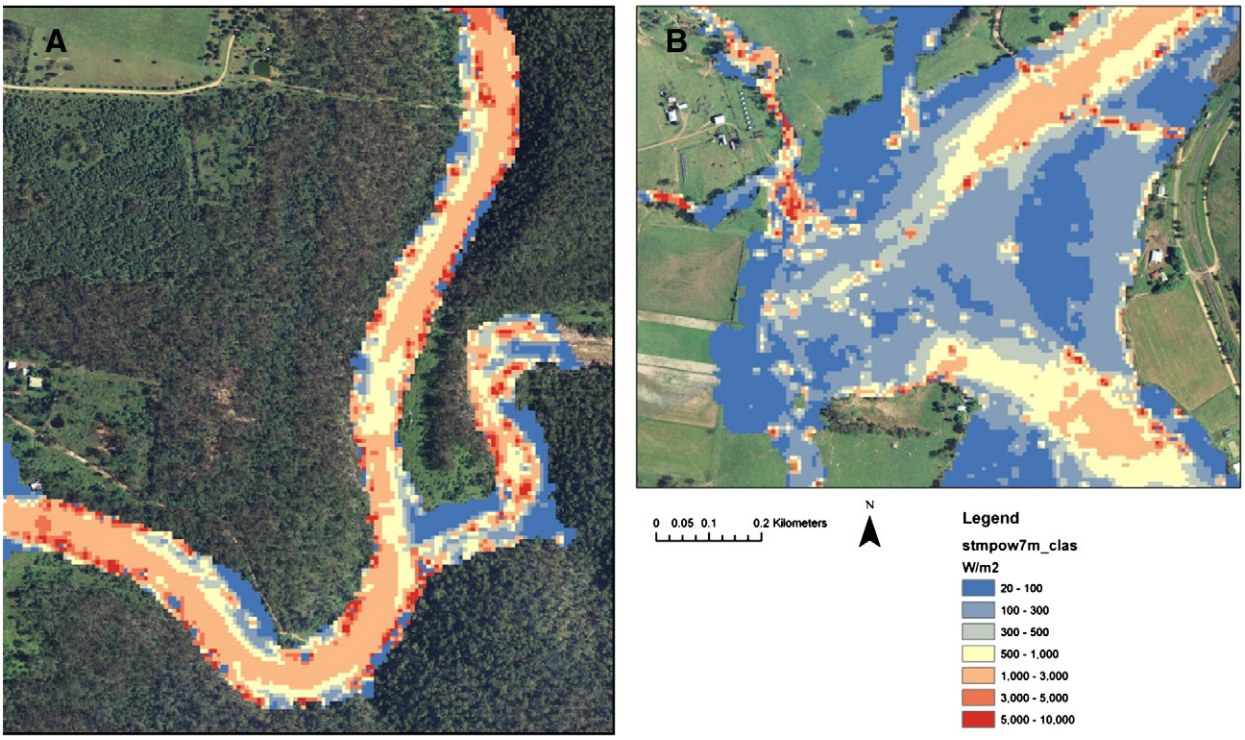

Fig. 6. Flood peak power modelled by TUFLOW for (A) a section of the confined reach and (B) part of the unconfined reach.

6. Discussion

Since the early work of Wolman and Miller (1960) and Leopold et al. (1964), the geomorphic importance of rare, high magnitude floods relative to flows of more moderate magnitude has been debated in fluvial geomorphology. This study provided the opportunity to investigate the geomorphic effects of an extreme flood that resulted in the loss of 22 lives and cost in excess of AU$3 billion in infrastructure damage in the Lockyer valley SEQ in January 2011. The predicted ARI of 2000 years places the event in the upper envelope of floods recorded in Australia. The availability of high resolution imagery and multitemporal LiDAR-derived DEMs used to construct an estimate of landscape change provided detailed data on the resultant geomorphic response.

6.1. Accuracy of the morphological budgeting approach and implications for key findings

Landscape change as a result of the 2011 flood was assessed here primarily in terms of the absolute and spatial patterns of erosion and deposition. Traditionally this would be achieved using channel planform or cross-sectional surveys, which often obscure the detailed spatial patterns and overall 'representativeness' of the reported change. Notable advances have been made recently in the use of multitemporal data sets to determine spatial patterns and associated volumes of morphological change (Lane, 1998; Brasington et al., 2000; Lane et al., 2003; Procter et al., 2010; Wheaton et al., 2010; Milan et al., 2011; Croke et al., 2013). Such studies confirm that virtually any process that produces a magnitude of geomorphic change larger than minimum detection limits has the potential to be studied using DEM differencing (Wheaton et al., 2010). More recent studies have also extended the application of the approach to larger spatial areas (Procter et al., 2010; Croke et al., 2013) and confirm its potential to make rapid and accurate assessments of landscape change at the basin scale.

Table 4
Modelled flood power for the January flood peak.

Reach	Feature	Unit stream power (W m^{-2})		Boundary shear stress (N m^{-2})	
		Mean	$+2\sigma$	Mean	$+2\sigma$
Confined	Inner channel	1877	4277	457	1151
	Inner channel banks	1732	3898	537	1709
	Bench	1742	4360	517	1557
	Macrochannel banks	2051	5971	1473	4657
	Floodplain	898	4052	543	2529
Unconfined	Inner channel	698	1754	233	543
	Inner channel banks	691	1961	263	765
	Bench	347	1361	150	612
	Macrochannel banks	698	2928	419	1887
	Floodplain	180	1180	116	760

The rapidly expanding use of DoD has also raised awareness of the need to assess the reliability of resultant erosion and deposition estimates. Elevation accuracy, which for airborne LiDAR has reported accuracies anywhere from ± 0.02 to ± 1 m (Fuller et al., 2003; Carter et al., 2007; Wheaton et al., 2010; Croke et al., 2013), is clearly important where estimates of morphological budgeting are required. The RMSE estimates of 0.08 m ($\pm 0.17\sigma$) for both LiDAR surfaces used in this study are fairly typical of the range of accuracies previously reported and reflect the aboveground bias of LiDAR. In the gross basin-scale analysis, Croke et al. (2013) used a minimum level of detection threshold of ± 0.23 m together with a conservative probabilistic estimate of 95% to eliminate areas of high uncertainty in the resultant DoD. This resulted in the interpretation of elevation differences in the interval ± 0.44 m as having a $>5\%$ probability of occurring by chance alone. Data in this basin-scale study were represented graphically using elevation change distributions (ECDs cf Wheaton et al., 2010) specifically to assess the proportion of elevation data within the five geomorphic features that lay within this error range. The magnitude of change reported across all geomorphic features had a range of almost 16 m, almost an order of magnitude higher than previous applications of DoD in gravel-bed environments; but the mean elevation change was 0.04 m ($\pm 0.32\sigma$), and up to 98% of the resultant data fell within

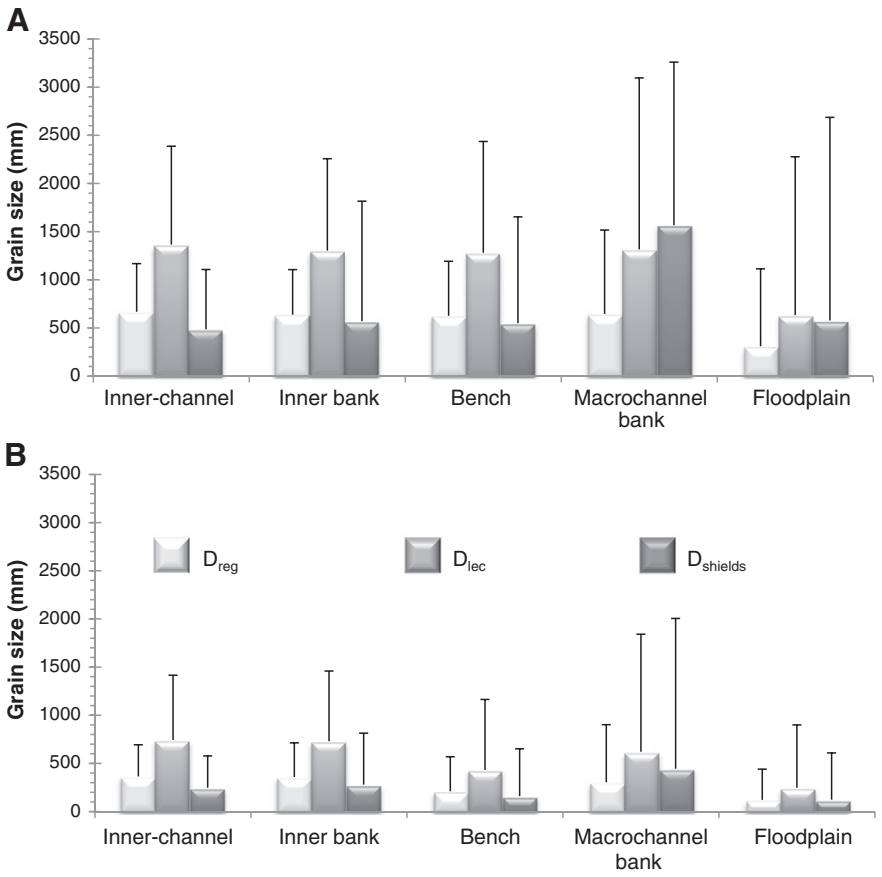

Fig. 7. Predicted flood competence across geomorphology types in (A) the confined reach and (B) the unconfined reach for Costa's linear regression equation (Eq. (3)), Costa's lower envelope curve (Eq. (4)) and Shield's equation (Eq. (5)).

the 95% critical limit of detection. However, this value was significantly influenced by the very large spatial area of floodplain (96 km^2) that experienced low magnitude change across large spatial areas and, even with ~98% of the data excluded, still contributed over 1 million m^3 of sediment deposition (Croke et al., 2013). At the basin-scale, error estimates varied across geomorphic features with the floodplain displaying the highest degree of uncertainty (Croke et al., 2013). Implications of the error-assessment reported in the basin-scale study are less relevant in terms of this study for several reasons. Firstly, the areal representation of floodplain in the two selected reaches is very small (0.7 km^2), <1% of that included in the basin-scale estimate. Secondly, the mean and range elevation changes on the floodplain of these reaches are 2–3 times higher than the overall basin-scale estimate, with some of the highest estimates of floodplain deposition reported for the entire basin. The use of a spatially average error, however, will result in some over- or underestimation of elevation changes in some parts of the DEM. Reported changes are best considered therefore as relative rather than absolute differences. In this study, relative magnitudes of change both within and between the study reaches are large with the unconfined reach showing elevation gains approximating to 70% of the material eroded from the upstream confined reach. The extraction of elevation difference data at a very fine (5-cm) resolution is also likely to contribute to a more accurate representation of elevation changes across geomorphic features than previously reported in other studies (Lane et al., 2003; Wheaton et al., 2010; Milan et al., 2011). This coupled with the use of a 1-D hydraulic model to estimate differences in the areal representation of pre- and post-flood geomorphic features represents one of the most accurate applications of morphological budgeting reported to date. However, as observed elsewhere (Fuller, 2008; Croke et al., 2013), the approach cannot differentiate the compensating effects of scour and fill, with erosion likely to occur during peak discharges and stream power and deposition during the falling limb and reduced energy. This may have implications for the estimates of erosion and deposition reported in both reaches but notably in the unconfined reach, which shows evidence of significant erosion in the form of a flood chute, and deposition across much of the downstream floodplain area. The extent to which estimates of deposition reflect the effects of reduced stream power during the latter stages of the event is largely unknown.

6.2. Flood magnitude

Whilst spectacular examples of large-scale channel and floodplain adjustment following extreme or catastrophic flood events have been described worldwide (Baker, 1973; Church, 1978; Costa, 1983; House et al., 2002), other studies reveal that such extreme events produced little geomorphic change (Costa and O'Connor, 1995; Magilligan et al., 1998). Floods of similar magnitude and frequency often result in dissimilar morphological responses even within the same catchment (Costa, 1974; Nanson, 1986; Costa and O'Connor, 1995; Fuller, 2008), and as a result it has remained difficult to predict the likely response of a catchment to a flood of a given magnitude or frequency.

The magnitude of the January 2011 Lockyer Creek flood is one of the largest recorded in Australia with specific peak (instantaneous) discharges relative to catchment area exceeding those published for the catastrophic 1949 flood on Wollombi Brook (4.14 $m^3\ s^{-1}\ km^{-2}$), the catastrophic 1971 Genoa River flood (5 $m^3\ s^{-1}\ km^{-2}$), the catastrophic 1993 Black Range Creek flood (6.71 $m^3\ s^{-1}\ km^{-2}$) (Erskine and Saynor, 1996), and the 1918 Pioneer Creek flood (6.6 $m^3\ s^{-1}\ km^{-2}$; Rodier and Roche, 1984). The magnitude of the January 2011 flood was

more than 10 times the MAF, which defines it as catastrophic (Erskine, 2011). In the context of world maximum rainfall-runoff floods and the envelope curve presented by Costa (1987), the January 2011 flood along the upper Lockyer is an order of magnitude smaller than what is possible (Fig. 8). In contrast to the other catastrophic events described above, however, this event occurred in a subcatchment that was well vegetated, particularly along the riparian zone, and as such the extrinsic threshold exceeded by the Lockyer flood is unlikely to have been exacerbated by the exceedence of an intrinsic threshold associated with land use clearing (cf. Erskine, 2011). The predicted ARI of >2000 years in the upper catchment around Helidon is admittedly based on relatively short gauging records (~30 years) and as such is likely to be an overestimate of flood frequency. Hydraulic modelling of flood magnitude in the channels near Helidon, however, confirm that bankfull discharge estimates of 5600 $m^3 s^{-1}$ are required to fill these channels to capacity with predicted recurrence intervals approaching the probable maximum flood (PMF) (Croke et al., in press). In spite of the significant magnitude of the January 2011 flood event, whole-of-valley flooding did not occur and the degree of flood inundation varied significantly between reaches downstream. Flood waters were fully contained within the bedrock-confined reach of Murphys Creek and it was not until Lockyer Sidings, the first available floodplain downstream in the unconfined reach, which floodwaters spilled out across the valley floor. Flood magnitude in the upper reaches of the catchment was intensified by the location of the storm cell that was focused primarily in the upper reaches of Murphys Creek and its adjacent tributaries of Fifteen Mile and Alice Creeks where maximum rainfall intensities and peak discharges were recorded (SKM, 2012). As documented here, the geomorphic response to the flood was significant in both reaches with notable changes in channel and floodplain extent and resultant estimates of erosion and deposition. Geomorphic response of floods is commonly assessed in terms of net erosion, and deposition is often overlooked in terms of its geomorphic significance. This study described how the dominance of either process can switch in adjacent but geomorphologically contrasting reaches.

6.3. Flood power

Previous research has shown that flood magnitude alone is a poor predictor of geomorphic 'work' and resultant landscape change during extreme flood events (Gardner, 1977; Magilligan, 1992; Kale, 2008). Baker and Costa's (1987) work highlighted the importance of flood power or energy whereby erosion and floodplain stripping are seen as the product of exceedence of some resistance threshold in the valley floor. Magilligan (1992) later quantified a minimum threshold for major morphological change using field and published data from extreme events and concluded that a threshold of 300 W m^{-2} was a good approximation. Flood power estimates for the January 2011 Lockyer Creek event peaked at ~9800 W m^{-2} with predicted mean flood power values within the macrochannel of the confined reach exceeding around six times the 300 W m^{-2} threshold postulated for morphological reworking of the channel (Magilligan, 1992). Thresholding the spatial distribution of TUFLOW modelled flood power at 300 W m^{-2} revealed that 74% of the area of the confined reached exceeded this threshold whilst 73% of the unconfined reach was below this value (Fig. 9A). The area of the confined reach not exceeding the threshold related to the main floodplain areas at the two meander bends and at the small tributary junctions, which were the main loci of deposition in this reach. There is a good agreement, therefore, between the spatial patterns of erosion and deposition recorded in both reaches and the predicted estimates of flood power (Fig. 9B). One notable exception to this pattern is the cutting of a flood chute in the unconfined reach at a location of low relative flood power. Field surveys at this site revealed a large log jam across the thalweg adjacent to the start of the flood chute. Flow deflection from the log jam at some point during the flood may have either initiated or exacerbated cutting of the flood chute, as has been described in other channels with high loadings of woody debris (e.g., Phillips, 2012). These stochastic elements were not accounted for in the hydraulic model and are difficult to incorporate into flood hazard modelling (Mazzorana et al., 2011).

The presence of high stream power values, and resultant high erosion rates, within the confined reach is a function of the higher energy gradient coincident with knickpoint development and channel steepening at ~18 km downstream. The location of this knickpoint is significant because it lies at a distance downstream that is theoretically described as having relatively high total and unit stream power for a conventional concave longitudinal profile stream (Knighton, 1999; Fonstad, 2003). Knickpoints occurring along rivers in the 10–100 km downstream distance range can produce extremely high unit stream power during floods that translate to river reaches exposed to potentially high morphological and ecological disturbances (Bendix, 1999; Thompson et al., 2008). This distance, or equivalent catchment area, contains the optimum tradeoff between decreasing energy gradient and accumulating catchment runoff (Knighton, 1999). In the case of the Lockyer, the presence of this knickpoint, together with the reaches' proximity to the headwaters that were strongly aligned to the source of the storm, resulted in the rapid onset and fast transmission of the flood peak. As channel gradient and flood power decreased, deposition replaced erosion as the dominant process. Notably, however, the unconfined reach also experienced significant erosion by way of a flood chute in spite of significantly reduced stream power suggesting that geomorphic response is not related to stream power alone, and additional factors at this site such as flow alignment and the reduced calibre of substrate across the bend apex are likely to have influenced spatial patterns of erosion.

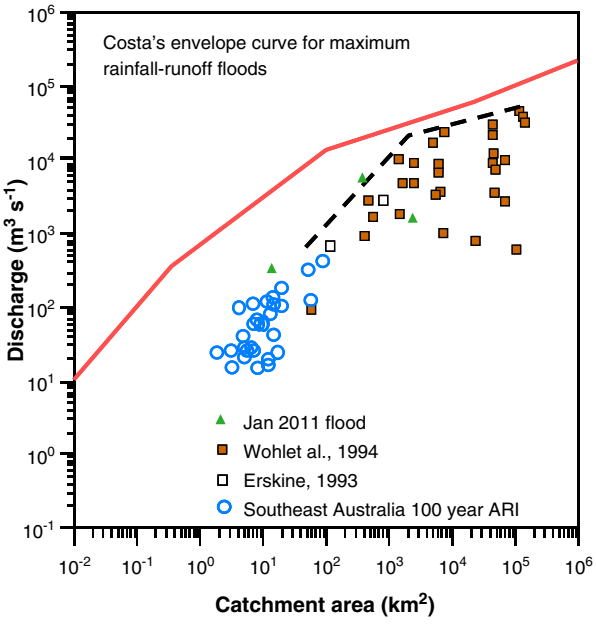

Fig. 8. Maximum rainfall-runoff flood curve of Costa (1987) with Australian flood peaks plotted.

6.4. Flood competence

Predicting flow competence even for low to moderate discharges is often problematic using empirically derived equations (Lorang and Hauer, 2003). Thompson and Croke (2008) for example reviewed the performance of eight channel competence equations in accurately predicting bedload transport for high energy bedrock streams in southeastern Australia and found that the equations overpredicted grain size entrainment because of the persistence of channel bed

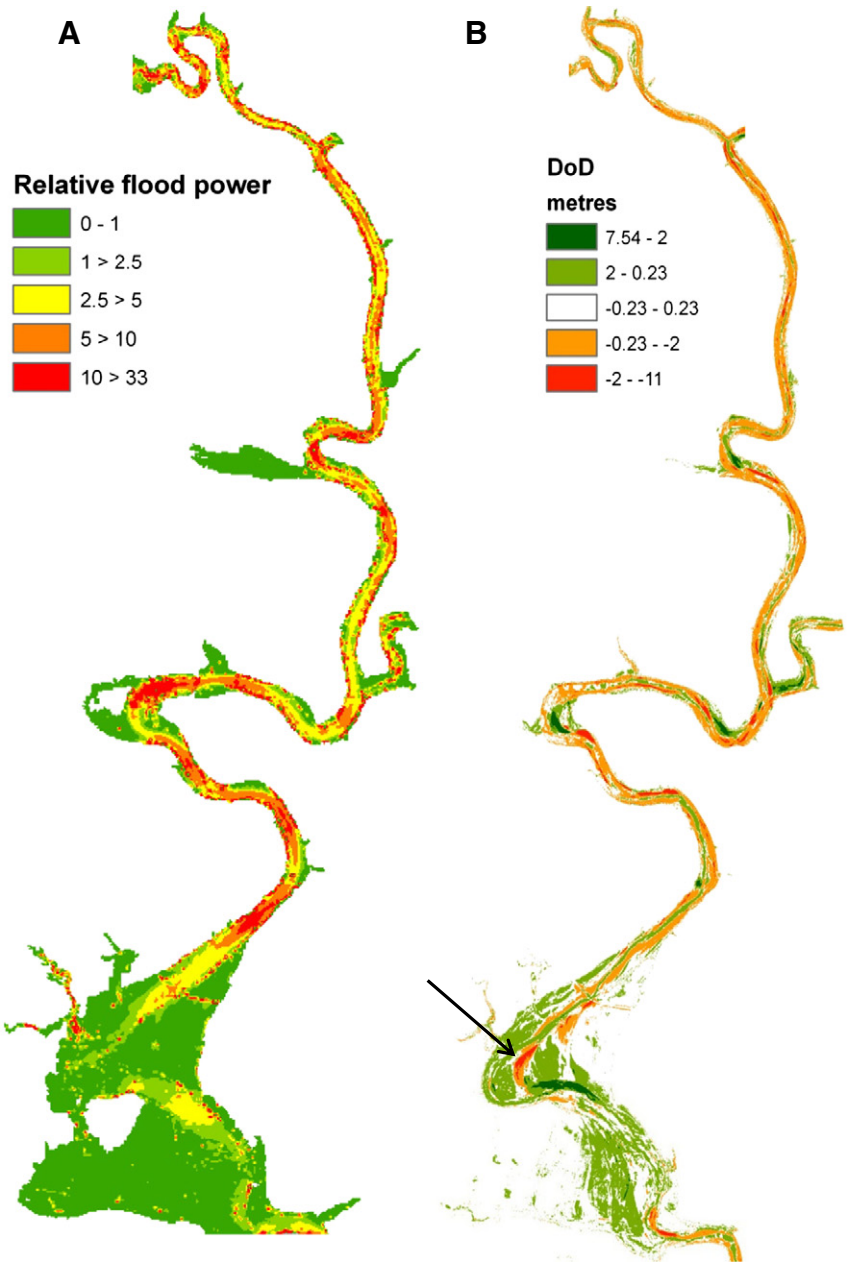

Fig. 9. A comparison of (A) January 2011 flood peak power relative to the proposed minimum power for effective geomorphic work, and (B) the DoD illustrating the major patches of erosion and deposition along the confined and unconfined reaches.

armoring. The application of these equations to predict competence during an extreme flood event is potentially more problematic as greater uncertainties exist in accurately parameterising both peak flow and channel boundary conditions. For example, all three competence equations used in this study assume Newtonian flow. However, given the extremely sudden onset of the flood (flash flood) combined with its extreme magnitude, the likelihood of hyperconcentrated or non-Newtonian flow conditions prevailing is high. Evidence for this is also suggested by a number of small landslides in the headwaters of tributaries, particularly Fifteen Mile Creek, and the amount of riparian vegetation stripped from within the macrochannel. Similar conditions have been reported during floods elsewhere (Batalla et al., 1999; Milan, 2012). In examples from the central Pyrenees and Bavarian Alps, reported rainfall intensities, wet antecedent conditions, and specific discharges of 20 $m^3\ s^{-1}\ km^{-2}$ were very similar to those reported for the Lockyer valley (Rogencamp and Barton, 2012). The flood wave velocity for the upper Lockyer is estimated at 4.4 $m\ s^{-1}$ with flow velocities significantly higher (ICA Hydrology Panel, 2011), which fall within the range for debris-type flows (Costa, 1984). However, the channel gradients are an order-of-magnitude less than those described producing hyperconcentrated flows and generally too low for debris-type flows (Costa, 1984). If hyperconcentrated flow did occur, then applying a Newtonian transport equation such as Shield's is likely to be inappropriate. The same could be argued for Costa's equations. Thompson and Croke (2008) found that, for small floods just exceeding bankfull capacity in southeast Australia, Costa's lower envelope curve (D_{lec} Eq. (4)) was too conservative and that Costa's linear regression (D_{reg}) predicted grain sizes closer to that measured in bedload traps. For these smaller floods, selective transport was the dominant process for the largest grains whilst smaller grains showed equal mobility (Thompson and Croke, 2008). However, given that Costa's equation is empirically derived from boulder deposits after extreme floods, it more than likely integrates both Newtonian and non-Newtonian conditions.

Therefore, Costa's lower envelope curve may be the most suitable competence equation for the catastrophic upper Lockyer flood, and it confirms that the boulders measured along the confined reach had most likely been transported during the flood rather than remnant boulders simply uncovered by the flood.

6.5. Spatial changes in valley configuration

Two reaches were selected in this study to assess differences in geomorphic responses owing to spatial changes in valley configuration. Dramatic differences in geomorphic responses were observed between the two reaches that were spatially adjacent to each other. The upstream bedrock-confined reach experienced large-scale erosion and reorganisation of the channel morphology, which resulted in significantly different areal representations of the five geomorphic features classified in this study. Most notable was the dramatic channel widening that occurred through lateral erosion along the margins of the channel and benches. In contrast, the downstream unconfined reach experienced negligible channel widening, and the reach was net depositional. Similar accounts of the effects of valley configuration on the geomorphic effectiveness of extreme flood events have been presented elsewhere. Fuller (2008), for example, documented similar contrasts in the behaviour and response of a 100-year flood event in New Zealand. Spatial changes in valley configuration remain an important factor in explaining geomorphic responses recorded elsewhere throughout the Lockyer catchment. For example, immediately below the unconfined reach, flood waters were concentrated again through a valley constriction; and this pattern of alternating confined and unconfined flow continued downstream to the township of Grantham (Fig. 1) where flood waters spilled out across the widened valley floor. The majority of lives were lost at this location as the depth and velocity of flood waters exceeded safety guidelines for masonry buildings and numerous dwellings located on the floodplain were destroyed (Rogencamp and Barton, 2012).

7. Conclusion

This study presented an assessment of the geomorphic effectiveness, magnitude, and effective energy of the January 2011 flood in the upper reaches of the Lockyer valley SEQ, Australia. The event stands as one of Australia's largest floods in terms of instantaneous discharge per unit area with estimated recurrence intervals ranging from 2000 years (headwaters) to 30 years (end of catchment) based on short gauging station records. The proximity of the study reaches to the source of the storm in the headwaters of the catchment led to very rapid and flash-flood-like conditions as rainfall intensities of >110 mm h^{-1} fell on an already saturated catchment. The presence of a recognised knickpoint within the confined reach is believed to have contributed to the high unit stream power values of 9800 W m^{-2} and subsequent catastrophic erosion throughout this reach. Further work is underway to date the preserved alluvial deposits, which can be used to reconstruct past flood magnitudes and frequency.

Acknowledgements

This project was supported by the Queensland's Department of Science, Information Technology, Innovation and the Arts (DSITIA) as part of the Flood Recovery Project 2011 and an Australian Research Council Linkage Award (LP120200093). We are particularly grateful to field crews from the Chemistry Centre, Land Resource Assessment and Remote Sensing in DSITIA who assisted in field data collection. Greg Rogencamp (SKM) provided assistance with the re-running of TUFLOW that was used in this study with permission from Lockyer Valley Council (LVC). The constructive comments of four anonymous reviewers and Editor Prof. Richard Marston were also gratefully appreciated.

References

Aggett, G.R., Wilson, J.P., 2009. Creating and coupling a high-resolution DTM with a 1-D hydraulic model in a GIS for scenario-based assessment of avulsion hazard in a gravel-bed river. Geomorphology 113, 21–34.
Andrews, E.D., 1983. Entrainment of gravel from naturally sorted riverbed material. Geological Society of America 94, 1225–1231.
Baker, V.R., 1973. Paleohydrology and sedimentology of Lake Missoula flooding in eastern Washington. Special Paper, 144. Geol. Soc. Am, Boulder, CO.
Baker, V.R., Costa, J.E., 1987. Flood power. In: Mayer, L., Nash, D. (Eds.), Catastrophic Flooding. Allen and Unwin, Boston, MA, pp. 1–24.
Baker, V.R., Kochel, R.C., Patton, P.C., 1988. Flood Geomorphology. John Wiley and Sons, New York.
Batalla, R.J., DeJong, C., Ergenzinger, P., Sala, M., 1999. Field observations on hyperconcentrated flows in mountain torrents. Earth Surface Processes and Landforms 24, 247–253.
Bathurst, J.C., 1978. Flow resistance of large-scale roughness. American Society of Civil Engineers, Journal of the Hydraulics Division 104, 1587–1603.
Bendix, J., 1999. Stream power influence on the southern Californian riparian vegetation. Journal of Vegetation Science 10, 243–252.
Brasington, J., Rumsby, B.T., McVey, R.A., 2000. Monitoring and modelling morphological change in a braided gravel-bed river using high resolution GPS-based survey. Earth Surface Processes and Landforms 25, 973–990.
Brasington, J., Langham, J., Rumsby, B., 2003. Methodological sensitivity of morphometric estimates of coarse fluvial sediment transport. Geomorphology 53, 299–316.
Brooks, A.P., Brierley, G.J., 1997. Geomorphic responses of lower Bega River to catchment disturbance, 1851–1926. Geomorphology 18, 291–304.
Bureau of Meteorology (BoM), 2012. Annual Australian Climate Statement 2010/2011. http://www.bom.gov.au/announcements/media_releases/climate/change/20120104.shtml.
Carter, W.E., Shrestha, R.L., Slatton, K.C., 2007. Geodetic laser scanning. Physics Today 60, 41–47.
Charlton, M.E., Large, A.R.G., Fuller, I.C., 2003. Application of airborne LiDAR in river environments: the River Coquet, Northumberland, UK. Earth Surface Processes and Landforms 28, 299–306.
Cheetham, M.D., Bush, R.T., Keene, A.K., Erskine, W.D., Fitsimmons, K.E., 2010. Longitudinal correlation of late Quaternary terrace sequences of Widden Brook, southeast Australia. Australian Journal of Earth Sciences 57, 97–109.
Church, M., 1978. Paleohydrological reconstructions from a Holocene valley fill. In: Miall, A.D. (Ed.), Fluvial Sedimentology: Can. Soc. Pet. Geol. Mem, 5, pp. 743–772.
Costa, J.E., 1974. Response and recovery of a Piedmont watershed from tropical storm Agnes, June 1972. Water Resources Research 10, 106–112.
Costa, J.E., 1983. Paleohydraulic reconstruction of flash-flood peaks from boulder deposits in the Colorado Front Range. Geological Society of America Bulletin 94, 986–1004.
Costa, J.E., 1984. Physical geomorphology of debris flows. In: Costa, J.E., Fleisher, P.J. (Eds.), Developments and Applications of Geomorphology. Springer, Heidelberg, Germany, pp. 286–317.
Costa, J.E., 1987. A comparison of the largest rainfall-runoff floods in the United States with those of the Peoples Republic of China and the world. J. Hydro. 96, 101–115.
Costa, J.E., O'Connor, J.E., 1995. Geomorphically effective floods. In: Costa, J.E., Miller, A.J., Potter, K.W., Wilcock, P.R. (Eds.), Natural and anthropogenic influences in fluvial geomorphology. Geophys. Monogr. Ser, 89. AGU, Washington, D.C., pp. 45–56. http://dx.doi.org/10.1029/GM089p0045.
Croke, J., Todd, P., Thompson, C., Watson, F., Denham, R., Giri, K., 2013. The use of multi-temporal LiDAR to assess basin-scale erosion and deposition following the catastrophic January 2011 Lockyer flood, SE Queensland, Australia. Geomorphology. http://dx.doi.org/10.1016/j.geomorph.2012.11.023.
Croke, J., Reinfields, I., Thompson, C., Roper, E., 2013. Macrochannels and their significance for flood-risk minimisation: examples from southeast Queensland and New South Wales, Australia. Stochastic Environmental Research and Risk Assessment. http://dx.doi.org/10.1007/s00477-013-0722-1(in press).
Erskine, W.D., 1993. Erosion and deposition produced by a catastrophic flood on the Genoa River, Victoria. Australian Journal of Soil and Water Conservation 6, 35–43.
Erskine, W.D., 2011. Geomorphic controls on historical channel planform changes on the lower Pages River, Hunter valley, Australia. Australian Geographer 42, 289–307.
Erskine, W.D., Saynor, M.J., 1996. Effects of catastrophic floods on sediment yields in southeastern Australia. In: Walling, D.E., Webb, B.W. (Eds.), Erosion and Sediment Yield: Global and Regional Perspectives: Proceedings of An International Symposium Held at Exeter, UK, From 15–19 July 1996. No. 236. IAHS, pp. 381–388.
Erskine, W.D., Warner, R.F., 1988. Geomorphic effects of alternating flood- and drought-dominated regimes on NSW coastal rivers. In: Warner, R.F. (Ed.), Fluvial Geomorphology of Australia. Academic Press, Sydney, pp. 223–242.
Erskine, W.D., Warner, R.F., 1998. Further assessment of flood- and drought-dominated regimes in south-eastern Australia. Australian Geographer 29, 257–261.
Ferguson, R.I., 2005. Estimating critical stream power for bedload transport calculations in gravel-bed rivers. Geomorphology 70, 33–41.
Fewtrell, T.J., Neal, J.C., Bates, P.D., Harrison, P.J., 2011. Geometric and structural river channel complexity and the prediction of urban inundation. Hydrological Processes 25, 3173–3186.
Fonstad, M.A., 2003. Spatial variation in the power of mountain streams in the Sangre de Cristo Mountains, New Mexico. Geomorphology 55, 75–96.
French, J.R., 2003. Airborne LIDAR in support of geomorphologic and hydraulic modelling. Earth Surface Processes and Landforms 28, 321–335.
Fuller, I.C., 2008. Geomorphic impacts of a 100-year flood: Kiwitea Stream, Manawatu catchment, New Zealand. Geomorphology 98, 84–95.

Fuller, I.C., Large, A.R.G., Charlton, M.E., Heritage, G.L., Milan, D.J., 2003. Reach-scale sediment transfers: an evaluation of two morphological budgeting approaches. Earth Surface Processes and Landforms 28, 889–903.
Gallant, J.C., Dowling, T.I., 2003. A multiresolution index of valley bottom flatness for mapping depositional areas. Water Resources Research 39, 1347.
Gardner, J.S., 1977. Some geomorphic effects of a catastrophic flood on the Grand River, Ontario. Canadian Journal of Earth Science 14, 2294–2300.
House, P.K., Webb, R.H., Baker, V.R., Levish, D.R., 2002. Ancient floods, modern hazards. Principles and Applications of Paleoflood Hydrology. Water Sci. Appl., 5. Am. Geophys. Union, Washington, DC, p. 385.
Hunter, N.M., Bates, P.D., N´eelz, S., Pender, G., Villanueva, I., Wright, N.G., Liang, D., Falconer, R.A., Lin, B., Waller, S., Crossley, A.J., Mason, D.C., 2008. Benchmarking 2D hydraulic models for urban flooding. Proceedings of the Institution of Civil Engineers, Water Management 161, 13–30.
Hydrology Panel, I.C.A., 2011. Flooding in the Brisbane River catchment, January 2011. Flooding in the Lockyer Regional Council LGA. Insurance Council of Australia, vol. 4. NSW, Sydney, p. 106 (http://www.insurancecouncil.com.au/issue-submissions/reports/qld-floods).
Jansen, J.D., 2006. Flood magnitude–frequency and lithologic control on bedrock river incision in post-orogenic terrain. Geomorphology 82, 39–57.
Jansen, J.D., Brierley, G.J., 2004. Pool-fills: a window to palaeoflood history and response in bedrock-confined rivers. Sedimentology 51, 901–925.
Jordan, P.W., 2011. Hydrological advice to commission of inquiry regarding 2010/11 Queensland floods. Toowoomba and Lockyer Valley Flash Flood Events of 10 and 11 January 2011: Sinclair Knight Merz Report, Brisbane, Qld., p. 83 (http://www.floodcommission.qld.gov.au).
Kale, V.S., 2008. A half-a-century record of annual energy expenditure and geomorphic effectiveness of the monsoon-fed Narmada River, central India. Catena 75, 154–163.
Kermode, S.J., Cohen, T.J., Reinfelds, I.V., Nanson, G.C., Pietsch, T.J., 2012. Alluvium of antiquity: polycyclic terraces in a confined bedrock valley. Geomorphology 139–140, 471–483.
Kiem, A.S., Franks, S.W., Kuczera, G., 2003. Multi-decadal variability of flood risk. Geophysical Research Letters 30, 1035.
Kirkup, H., Brierley, G., Brooks, A., Pitman, A., 1998. Temporal variability of climate in south-eastern Australia: a reassessment of flood- and drought-dominated regimes. Australian Geographer 29, 241–255.
Knighton, D., 1999. Downstream variation in stream power. Geomorphology 29, 293–306.
Knox, J.C., 1993. Large increases in flood magnitude in response to modest changes in climate. Nature 361, 430–432.
Knox, J.C., 2000. Sensitivity of modern and Holocene floods to climate change. Quaternary Science Reviews 19, 439–457.
Komar, P.D., 1987. Selective gravel entrainment and the empirical evaluation of flow competence. Sedimentology 34, 1165–1176.
Lane, S.N., 1998. The use of digital terrain modelling in the understanding of dynamic river systems. Landform Monitoring, Modelling and Analysis. Wiley, Chichester, UK.
Lane, S.N., Westaway, R.M., Hicks, D.M., 2003. Estimation of erosion and deposition volumes in a large, gravel-bed, braided river using synoptic remote sensing. Earth Surface Processes and Landforms 28, 249–271.
Leopold, L.B., Wolman, M.G., Millar, J.P., 1964. Fluvial Processes in Geomorphology. W.H. Freeman and Company, San Francisco, CA (522 pp.).
Lorang, M.S., Hauer, F.R., 2003. Flow competence and streambed stability: an evaluation of technique and application. Journal of the North American Benthological Society 22, 475–491.
Macklin, M.G., Lewin, J., 2003. River sediments, great floods and centennial-scale Holocene climate change. Journal of Quaternary Science 18, 101–105.
Magilligan, F.J., 1992. Thresholds of spatial variability of flood power during extreme floods. Geomorphology 5, 373–390.
Magilligan, F.J., Phillips, J.D., James, L.A., Gomez, B., 1998. Geomorphic and sedimentological controls on the effectiveness of an extreme flood. Journal of Geology 106, 87–95.
Mazzorana, B., Comiti, F., Volcan, C., Schere, C., 2011. Determining flood hazard patterns through a combined stochastic-deterministic approach. Natural Hazards 59, 301–316.
Milan, D.J., 2012. Geomorphic impact and system recovery following an extreme flood in an upland stream: Thinhope Burn, northern England, UK. Geomorphology 138, 319–328.
Milan, D.J., Heritage, G.L., Large, A.R.G., Fuller, I.C., 2011. Filtering spatial error from DEMs: implications for morphological change estimation. Geomorphology 125, 160–171.
Nanson, G.C., 1986. Episodes of vertical accretion and catastrophic stripping: a model of disequilibrium flood-plain development. Geological Society of America 97, 1467–1475.
Nott, J., Price, D., 1999. Waterfalls, floods and climate change: evidence from tropical Australia. Earth and Planetary Science Letters 171, 267–276.
Phillips, J.D., 2002. Geomorphic impacts of flash flooding in a forested headwater basin. Journal of Hydrology 269, 236–250.
Phillips, J.D., 2012. Log-jams and avulsions in the San Antonio River Delta, Texas. Earth Surface Processes and Landforms 37, 936–950.
Pickup, G., Marks, A., Bourke, M., 2002. Paleoflood reconstruction on floodplains using geophysical survey data and hydraulic modeling. In: House, P.K., Webb, R.H., Baker, V.R., Levish, D.R. (Eds.), Ancient Floods, Modern Hazards, Principles and Applications of Paleoflood Hydrology. Water Sci. Appl., 5. Am. Geophys. Union, Washington, DC, pp. 47–60.
Procter, J., Cronin, S.J., Fuller, I.C., Manville, V., Lube, G., 2010. Quantifying the geomorphic impacts of a lake-breakout lahar from Mt Ruapehu, New Zealand. Geology 38, 67–70.
Rodier, J.A., Roche, M., 1984. World catalogue of maximum observed floods. IAHS-AISH Publication No. 143, Wallingford, UK. (354 pp.).
Rogencamp, G., Barton, J., 2012. The Lockyer Creek flood of January 2011: what happened and how should we manage hazard for rare floods. 52nd Annual Floodplain Management Association Conference (http://www.floodplainconference.com/papers2012.php).
Rustomji, P., Bennett, N., Chiew, F., 2009. Flood variability east of Australia's Great Dividing Range. Journal of Hydrology 374, 196–208.
SKM, 2012. Lockyer creek flood risk management study. Sinclair Knight Merz, Brisbane, Qld., vol. 1.
Sun, X., Thompson, C.J., Croke, B., 2011. Using a logistic regression model to delineate channel network in southeast Australia. In: Chan, F. (Ed.), International Congress on Modelling and Simulation (MODSIM 2011). Modelling and Simulation Society of Australia and New Zealand Inc., Australia, pp. 1916–1922.
Sun, X., Thompson, C.J., Croke, B.F.W., 2012. Use of the LiDAR elevation data to map channel continuity in Southeast Australia. In: Webb, A., Bonell, M., Bren, L., Lane, P.N.J., McGuire, D., Neary, D.G., Nettles, J., Scott, D.F., Stednick, J., Wang, Y. (Eds.), Proceedings of IUGG Workshop Revisiting Experimental Catchment Studies in Forest Hydrology, Melbourne, 353. IAHS Publication, Wallingford, UK, pp. 33–41.
Syme, W.J., Apelt, C.J., 1990. Linked two-dimensional/one-dimensional flow modelling using the shallow water equations. The Institution of Engineers Australia Conference on Hydraulics in Civil Engineering, Sydney, 3–5 July 1990. Australia Institute of Engineers, Barton, A.C.T, pp. 28–32.
Taylor, J., 1997. An Introduction to Error Analysis: The Study of Uncertainties in Physical Measurements. University Science Books, Sausalito, CA.
Thompson, C.J., Croke, J.C., 2008. Channel flow competence and sediment transport in upland streams in southeast Australia. Earth Surface Processes and Landforms 33, 329–352.
Thompson, C.J., Croke, J.C., Takkan, I., 2008. A catchment-scale model of mountain stream channel morphologies in southeast Australia. Geomorphology 95, 119–144.
Warner, R.F., 1997. Floodplain stripping: another form of adjustment to secular hydrological regime change in southeast Australia. Catena 30, 263–282.
Wheaton, J.M., Brasington, J., Darby, S.E., Sear, D.A., 2010. Accounting for uncertainty in DEMs from repeat topographic surveys: improved sediment budgets. Earth Surface Processes and Landforms 35, 136–156.
Whitaker, W.G., Green, P.M., 1980. Moreton Bay geology 1:250 000 series. Geological Survey of Queensland, Qld.Dept. Mines, Australia.
Wohl, E.E., 1992. Bedrock benches and boulder bars: floods in the Burdekin Gorge of Australia. Geological Society of Australia 104, 770–778.
Wolman, M.G., Miller, J.P., 1960. Magnitude and frequency of forces in geomorphic processes. Journal of Geology 68, 54–74.